Pergamon

Geochimica et Cosmochimica Acta, Vol. 61, No. 2, pp. 251–263, 1997

0016-7037/97 $17.00 + .00

PII S0016-7037(96)00326-2

Lead adsorption at the calcite-water interface: Synchrotron X-ray standing wave and X-ray reflectivity studies

NEIL C. STURCHIO,[1] RONALD P. CHIARELLO,[1] LIKWAN CHENG,[1,2] PAUL F. LYMAN,[2] MICHAEL J. BEDZYK,[1,2] YONGLIN QIAN,[1,2] HOYDOO YOU,[1] DENNIS YEE,[3] PHILLIP GEISSBUHLER,[3] LARRY B. SORENSEN,[3] YONG LIANG,[4] and DONALD R. BAER[4]

[1]Argonne National Laboratory, Argonne, Illinois 60439, USA
[2]Northwestern University, Evanston, Illinois 60208, USA
[3]University of Washington, Seattle, Washington 98195, USA
[4]Pacific Northwest National Laboratory, Richland, Washington 99352, USA

(*Received August* 7, 1996; *accepted in revised form September* 6, 1996)

Abstract—By combining synchrotron X-ray standing wave (XSW) measurements with synchrotron X-ray reflectivity measurements, we have determined: (1) the precise three-dimensional location within the calcite unit cell of submonolayer Pb ions adsorbed at the calcite (104) surface from dilute aqueous solutions, and (2) the precise one-dimensional location of these unit cells relative to the calcite surface. Our XSW measurements, using three separate calcite Bragg reflections for triangulation, show that most adsorbed Pb ions occupy Ca sites in the calcite lattice with an ordered coverage of 0.05 equivalent monolayers, while the remaining Pb ions are disordered with a coverage of 0.03 equivalent monolayers. Our X-ray reflectivity measurements show that the ordered Pb ions occur primarily (>70%) in the surface atomic layer of calcite. Atomic force microscopy (AFM) was used to characterize the topography of the calcite (104) surface under conditions similar to the X-ray experiments. The quantitative morphological information obtained by AFM was used to develop realistic models of the calcite surface. The calculated X-ray reflectivities for these model surfaces were compared with the measured X-ray reflectivities. The new combined X-ray method that we have developed can be used to determine the atomic-scale structure of other metals adsorbed at mineral-water interfaces. Such high-resolution structural determinations are essential before detailed conceptual and theoretical models can be further developed to understand and predict the behavior of dissolved metals in mineral-water systems. *Copyright © 1997 Elsevier Science Ltd*

1. INTRODUCTION

Chemical and physical interactions at mineral surfaces control the transport behavior and bioavailability of hazardous metal contaminants and radionuclides in soils and groundwater systems (Hochella and White, 1990; Stumm, 1992; Vaughan and Pattrick, 1995). Atomic-scale structural information on metal speciation and reaction mechanisms at the mineral-water interface is required to achieve a fundamental understanding of these interactions. Recently, synchrotron X-ray standing wave (XSW) and X-ray reflectivity techniques have been shown to be particularly useful for in situ mineral-water interface studies on single-crystal substrates (Qian et al., 1994; Chiarello and Sturchio, 1994, 1995). In this paper we show that the combination of these two techniques can uniquely determine the position and quantity of Pb ions adsorbed at the calcite-water interface. The choice of Pb in this experiment was based on its importance as an environmental contaminant. It also has favorable X-ray characteristics (energy of X-ray absorption edge, high fluorescence yield, minimal Pb background in X-ray spectrum, high electron density) that maximize the sensitivity of the X-ray techniques. Calcite was chosen for its geochemical importance. It is also available in large, near-ideal, single crystals required for the X-ray techniques as performed at second-generation synchrotron facilities.

Despite the importance of studying Pb in the environment, there are few atomic-scale studies of the adsorption of Pb on minerals. Lead is one of the most common, toxic, heavy metal contaminants in the environment. Lead ingestion poses a severe threat to human health, and thus its environmental behavior is important to understand (Nriagu, 1978). Lead sorption to oxide mineral surfaces has been observed in powder sorption experiments and modeled using a surface complexation approach (Davis and Kent, 1990). Atomic-scale structural information for adsorbed Pb from X-ray absorption fine structure (XAFS) is available for Al and Fe-Mn oxides and hydrous oxides (Chisholm-Brause et al., 1990; Roe et al., 1991; Manceau et al., 1992) and for soils (Manceau et al., 1996). These XAFS studies have shown that Pb has a complicated coordination chemistry, but it generally forms monodentate or bidentate inner-sphere complexes with oxide surfaces at low coverage (submonolayer), and may form small multinuclear Pb complexes at higher coverage (near monolayer and above). In contrast, our study shows that most of the Pb adsorbed on calcite occupies the Ca site in the calcite surface.

Calcite is an important mineral that is ubiquitous in soils, shallow groundwater aquifers, and marine sediments. Its presence buffers the pH, pCO_2, and solute composition of porewaters (Stumm and Morgan, 1981). Calcite may be the dominant sorbent for a variety of metals in carbonate aquifers (Davis et al., 1987; Fuller and Davis, 1987; Zachara et al., 1991). Although limited information about Pb sorption on calcite is available, powder sorption experiments have shown

that divalent Mn, Co, Ni, Zn, and Cd cations are strongly sorbed by the calcite surface, whereas Sr and Ba are weakly sorbed by the calcite surface (e.g., Lorens, 1981; McBride, 1980; Davis et al., 1987; Zachara et al., 1988, 1991; Tesoriero and Pankow, 1996; Reeder, 1996). The strongly-sorbed group of cations have solid-liquid distribution coefficients greater than unity, ionic radii less than or approximately equal to that of divalent Ca (0.99 Å), are miscible in calcite, and form anhydrous carbonates having the calcite structure. The weakly-sorbed group of cations have solid-liquid distribution coefficients less than unity, ionic radii larger than divalent Ca, are immiscible in calcite, and form anhydrous carbonates having aragonite structure (Reeder, 1983; Zachara et al., 1991). The sorption behavior of the strongly-sorbed cations on calcite can be modeled closely by a surface exchange reaction, for which the detailed molecular mechanism is unknown. By the criteria outlined above, divalent Pb would be expected to behave like the weakly-sorbed cations Sr and Ba, because of its large ionic radius (1.20 Å) relative to that of Ca. Previously published studies of Pb sorption on calcite, however, were not designed to prevent the precipitation of Pb-bearing solid phases. Therefore, although significant sorption of Pb was observed in these experiments, it was not possible from the data obtained to make a clear distinction between adsorption and coprecipitation (Pickering, 1983; Fulghum et al., 1988; Wouters et al., 1988). The results of our study indicate clearly, however, that Pb adsorbs onto calcite and that the Pb ions go into Ca sites, despite the large ionic radius of Pb relative to Ca.

Atomic-scale structural data for adsorbates at the calcite-water interface are relatively scarce. Stipp et al. (1992) presented ex situ X-ray photo-electron spectroscopy (XPS), low energy electron diffraction (LEED), and Auger electron spectroscopy (AES) evidence for adsorption of one to four monolayers of Cd and for the epitaxial growth of otavite on a calcite cleavage surface that had been reacted with a Cd-bearing solution. They interpreted some of their data to indicate diffusion of Cd into the calcite lattice. Xu (1993) presented XAFS evidence for the formation of a $CoCO_3/CaCO_3$ solid-solution phase at the calcite-water interface. The locations of trace Sr and SeO_4 in the bulk calcite structure have also been studied using XAFS, indicating substitution of Sr for Ca (Pingitore et al., 1992) and SeO_4 for CO_3 (Reeder et al., 1994). Qian et al. (1994) used the XSW technique to show ex situ that Mn substitutes for Ca in the calcite lattice and that Pb sorbed from aqueous solution apparently occupies Ca sites within (104) lattice planes. The ex situ results of Qian et al. (1994), however, could not answer the question of which specific (104) lattice planes the Pb occupied near the calcite surface (i.e., whether Pb occurred in the surface layer only, in an adlayer above the surface, in one or more layers below the surface, or in any combination of these possibilities). Also, the XSW measurements of Qian et al. (1994) were limited to the (104) reflection and thus could not resolve the in-plane position of the Pb ions.

The present study used a combination of XSW measurements and X-ray reflectivity measurements to determine the specific position of Pb ions at the calcite-water interface. We used ex situ XSW measurements to triangulate the location of the Pb ions, verifying in three dimensions that they occupied Ca sites in the calcite lattice. We performed in situ XSW measurements, yielding results that are indistinguishable from the ex situ results. We also performed in situ X-ray reflectivity measurements, indicating that the Pb ions occurred primarily in the surface layer of calcite rather than above or below the surface. In addition to the X-ray measurements, we also used AFM to characterize the topography of the calcite surface under conditions similar to the X-ray experiments. The quantitative morphological information obtained by AFM was used to examine the validity of the models employed in calculating the X-ray reflectivity intensities. The combination of XSW and X-ray reflectivity measurements represents a powerful new approach for probing the atomic-scale structure of mineral-water interfaces. Structural information at this scale is needed for a fundamental understanding of reaction mechanisms and transport behavior in mineral-water systems.

2. X-RAY TECHNIQUES

This section provides a brief introduction to some of the X-ray techniques that have been shown to be useful for in situ mineral-water interface studies. Special attention is given to the two techniques, XSW and X-ray reflectivity, that were used in this study. The special combination of XSW and X-ray reflectivity measurements described in this paper has not been applied to other systems.

2.1. X-ray Absorption Spectroscopy

X-ray absorption spectroscopy (XAS) has been established as a useful set of techniques for in situ studies (see review by Brown et al., 1995). X-ray absorption fine structure (XAFS) can give quantitative information about the short-range atomic order around a specific adsorbate on the surface of a mineral (e.g., number and identity of nearest and next-nearest neighbors, bond lengths and angles), and X-ray absorption near-edge structure (XANES) can indicate the local coordination geometry and oxidation state of an adsorbate (Brown et al., 1995). Although generally used on powders and pastes, XAFS techniques can also be useful for surface-sensitive in situ studies of low-coverage adsorbates on single crystals when performed in a glancing-incidence geometry (Towle et al., 1993). However, the best surface sensitivity that can be obtained with glancing-incidence XAS is only about 100 Å.

2.2. X-Ray Standing Wave Measurements

The XSW technique was first applied to surfaces to determine the atomic positions and arrangement of adsorbed heavy ions relative to the lattice planes of nearly perfect silicon and germanium single crystals (Cowan et al., 1980; Golovchenko et al., 1982). XSW measurements can be done in various scattering geometries. In the standard Bragg diffraction geometry used in this study, the interference between the incoming and outgoing waves gives rise to a short

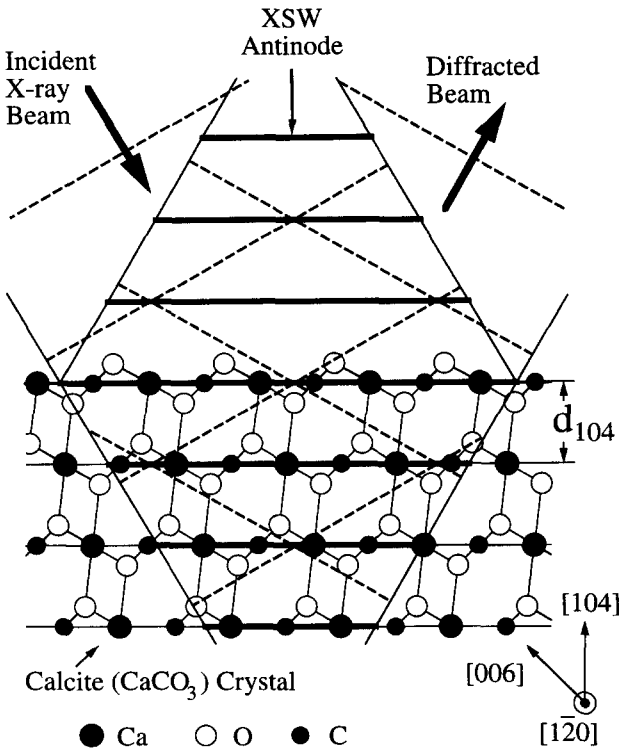

Fig. 1. Schematic diagram showing the XSW field generated by the Bragg diffraction from the calcite (104) lattice planes. The diffraction plane spacing d_{104} is 3.034 Å. On the high-angle side of the rocking curve, the antinodal planes of the XSW are aligned with the (104) diffraction planes, as shown. On the low-angle side, the nodes are aligned with the (104) planes. When the antinodes (nodes) of the XSW field are centered on the Pb ions in the Ca sites, the XSW field produces the maximum (minimum) fluorescence from the Pb ions. The Pb fluorescence intensity versus the XSW location is used to locate the Pb ions.

period (several Å) standing wave field (Fig. 1). This type of XSW experiment requires a nearly perfect crystal, and calcite is one of the few minerals available as nearly perfect single crystals. For imperfect crystals, a backscattering (90°) geometry can be used to generate the standing wave field. In this geometry, the incident X-ray wavelength is fixed at twice the lattice spacing. For typical mineral lattice d-spacings (2.5–10 Å), the incident beam energies (1–4 keV) required for XSW measurements in the backscattering geometry are too low for in situ studies, but they are useful for ultrahigh vacuum studies of oxide surface structures (Kendelewicz et al., 1995). A third type of XSW experiment can be performed with the use of layered synthetic microstructures (LSM), and the period of the standing wave can be controlled by the d-spacing of the LSM. This approach has proven to be appropriate for in situ studies of the structure of ultrathin organic films and electrochemical interfaces (Bedzyk et al., 1988). Finally, long-period standing waves (seventy to thousands of Å) can be generated by total external reflection from high quality X-ray mirrors. For example, the ion distribution in the diffuse double layer at an electrified interface and the structure of Langmuir-Blodgett films up to 1000 Å thick have been studied in situ by using XSW generated by total external reflection (Bedzyk et al., 1990; Wang et al., 1991).

From the von Laue and Ewald dynamical theory of X-ray diffraction, it has been shown that an XSW is generated within a perfect single crystal and extends above its surface during Bragg diffraction (Batterman and Cole, 1964; Batterman, 1969; Cowan et al., 1980). The period of the XSW is equal to the d-spacing of the diffraction planes, and its antinodes can be shifted relative to the diffraction planes by rocking the crystal in angle θ (or by scanning the incident beam energy at fixed angle) through the arcsecond wide Darwin curve of a strong Bragg reflection (see Fig. 1). By monitoring the modulation of the fluorescence yield from a specific atomic species vs. the XSW phase, one can determine the atomic position (or distribution) relative to the bulk diffraction plane. The fluorescence yield varies as a function of angle θ according to the following equation:

$$Y(\theta) = Y_{OB}\,[1 + R(\theta) + 2\sqrt{R(\theta)}\,f_H \cos(\nu(\theta) - 2\pi P_H)] \quad (1)$$

where Y_{OB} is the off-Bragg fluorescence yield. The reflectivity $R(\theta)$ and the XSW phase $\nu(\theta)$ are derived from dynamical diffraction theory. The coherent fraction f_H and the coherent position P_H represent the amplitude and phase of the H^{th} Fourier component of the spatial distribution of the atomic species. The coherent position is the $\Delta d/d$ fractional position ranging from 0–1, where 0 and 1 correspond to adjacent diffraction planes and 0.5 corresponds to a position halfway between the diffraction planes. The coherent fraction, which also ranges from 0–1, measures the static and dynamic spread of the atomic distribution. The parameters f_H and P_H are obtained from a χ^2 fit of Eqn. 1 to the XSW data after background subtraction. Uncertainties in f_H and P_H are typically ±0.03 and ±0.02, respectively, based on counting statistics and a sensitivity analysis of the fitting procedure.

XSW measurements performed in the Bragg scattering geometry can precisely determine the position of the adsorbed ions inside the unit cell but cannot determine the location of the unit cells containing the adsorbed ions to better than about 1000 Å. The absorption of the primary X-ray field and the absorption of the secondary X-ray emission in the crystal affects the shape of the X-ray standing wave fluorescence signal. This effect is clearly visible when, for example, the element is uniformly distributed through the volume of crystal that interacts with the X-rays (Bedzyk and Materlik, 1985; Qian et al., 1994). For the calcite (104) reflection, the X-ray extinction depth is about 0.7 μ (Qian et al., 1994). Therefore, if the adsorbate is within about 1000 Å of the surface, its fluorescence signal will be indistinguishable from an atom at the surface. Thus, XSW measurements cannot tell which specific atomic layer contains the atom. Consequently, we used XSW to determine where the Pb ions were located inside the unit cell, and we used X-ray reflectivity to determine where the unit cells containing the Pb ions were located with respect to the surface of the crystal.

2.3. Specular X-Ray Reflectivity

Recently, X-ray reflectivity measurements have been shown to provide important information about in situ min-

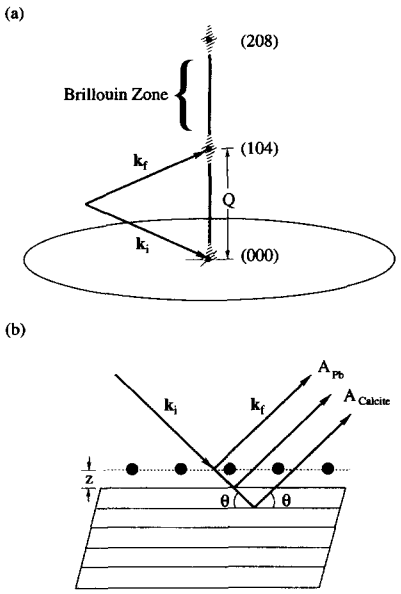

Fig. 2. The geometry of specular X-ray reflectivity in reciprocal space and in real space. (a) Schematic illustration of the specular crystal truncation rod (CTR) in reciprocal space. The CTR is produced by the truncation of the surface and it connects the bulk (000), (104), and (208) Bragg reflections. The first Brillouin zone extends from the (000) reflection to the (104) reflection; the second zone from the (104) to the (208) reflection, and the third zone from the (208) to the (3, 0, 12) reflection. The CTR intensity falls to a minimum near the middle of each Brillouin zone and is very sensitive to the detailed atomic structure of the interface. (b) Schematic illustration of the specular X-ray reflectivity in real space for a calcite single crystal with a submonolayer of Pb adsorbed on its surface. The total specularly reflected intensity is produced by the interference between the reflection from the Pb layer, located at position z relative to the crystal surface, and the combined reflection from all of the calcite layers. For the specular reflection the angle of incidence is equal to the angle of reflection, and the wavevector transfer $\mathbf{Q} = k_f - k_i$ is perpendicular to the interface and its magnitude is given by $\mathbf{Q} = (4\pi/\lambda) \sin(\theta)$, where θ is the angle of incidence and reflection and λ is the X-ray wavelength.

eral-water interfaces (Chiarello et al., 1993; Chiarello and Sturchio, 1994, 1995). Although it has long been established in classical X-ray crystallography that the intensities of the Bragg peaks directly measure the magnitudes of the Fourier components of the electron density of the crystal, it was only appreciated relatively recently that the reflection from the surface produces rods of intensity (see Fig. 2a) that provide important information about the surface structure of the crystal (Andrews and Cowley, 1985; Robinson, 1986). These rods, which are perpendicular to the interface, are often referred to as crystal truncation rods (CTRs), and are sensitive to the Fourier transform of the electron density near the surface. At the Bragg peaks, the reflected X-ray intensity arises from the long-range order within the crystal. Between the Bragg peaks, the CTR intensity falls to a minimum near the center of the Brillouin zone and is very sensitive to the detailed atomic structure of the interface. This is because almost all of the scattered waves from the interior atoms interfere destructively in the middle of the Brillouin zone. Consequently, adsorbate atoms with a well-defined position z relative to the surface will produce a substantial contribution to the total intensity of the Brillouin zones between the Bragg peaks. These CTR intensities provide important information with submonolayer sensitivity on the atomic structure of the surface, including: (1) surface reconstructions, (2) surface relaxations, (3) surface roughness, and (4) disordered surface phases (Als-Nielsen, 1991; Toney et al., 1994; Chiarello and Sturchio, 1995).

Specular X-ray reflectivity measurements can be used to determine the position z of an adsorbed monolayer relative to the substrate surface because the intensity of the specular reflectivity depends on the interference between the adsorbate and the substrate scattering (see Fig. 2b). In specular reflectivity, the angle of incidence is equal to the angle of reflection and the wavevector transfer $\mathbf{Q}$ is perpendicular to the interface. To ensure uniform sampling in reciprocal space, our data is actually recorded and analyzed in terms of the wavevector transfer, $\mathbf{Q} = (4\pi/\lambda) \sin(\theta)$, rather than in terms of the angle θ. Specular reflectivity is only sensitive to the projection of the electron density onto the direction perpendicular to the interface. When there is a complete monolayer of the adsorbed species, specular reflectivity alone can be used to accurately determine the adsorbate position z. In the present experiments, we wanted to determine the location of a submonolayer of Pb ions at the calcite-water interface. Since there is only 5% of a monolayer of Pb, the interference signal is twenty times smaller than the interference signal that would be produced by a complete monolayer of Pb. Consequently, it is difficult to determine the precise position z using only specular X-ray reflectivity. However, because the XSW measurements show that the Pb ions are in Ca sites in the lattice, we know that the position z is equal to zero, modulo an integer multiple of the 3.0 Å d-spacing of the calcite (104) lattice planes. The interference signal from 5% of a monolayer of Pb is strong enough to allow us to determine the location of the Ca sites that contain the Pb ions to within one calcite (104) layer.

To determine the position z of the adsorbed Pb ions relative to the calcite surface, we must analyze the difference between the specular reflectivity of the calcite surface with and without any adsorbed Pb. The intensities of the specular reflectivity of the calcite-water interface and of the calcite-Pb-water interface are given, respectively, by

$$I_{\text{calcite}}(\mathbf{Q}) \propto |A_{\text{calcite}}(\mathbf{Q})|^2 \quad (2)$$

$$I_{\text{calcite+Pb}}(\mathbf{Q}) \propto |A_{\text{calcite}}(\mathbf{Q}) + A_{\text{Pb}}(\mathbf{Q})|^2 \quad (3)$$

Note that the measured intensities depend on the scattering amplitudes for the reflected X-ray waves from the calcite-water interface $A_{\text{calcite}}(\mathbf{Q})$ and from the Pb-bearing layer, $A_{\text{Pb}}(\mathbf{Q})$. Because these amplitudes are complex, i.e., they have both an amplitude and a phase, we need to know the magnitude and the phase of both scattering amplitudes before we can calculate the two intensities. To determine $A_{\text{calcite}}(\mathbf{Q})$, we made two different models of the atomic structure of the calcite-water interface. In the first model, we assumed that the calcite surface was ideally truncated, but we let the oxygen atoms in the two surface layers relax. In the second model, we added two partial layers to the surface of the calcite, and we let the oxygen atoms in the surface layer and

Table 1. Initial solution compositions[a].

	Solution 1	Solution 2	Solution 3[b]
pH	8.78	9.11	8.18
Na	255	239	35.6
Ca	1.75	1.07	31.0
Pb	16.6	22.7	2.05
HCO_3[c]	580	610	177
Cl	18.5	8.7	7.12
EDTA	48	54	4.38
I[d] (M)	0.008	0.010	0.0028

[a] concentrations in mg/L
[b] solution used by Qian et al. (1994)
[c] total alkalinity as HCO_3
[d] ionic strength

in the two partial layers relax. We fit these two models to the measured $I_{calcite}(\mathbf{Q})$ to determine $A_{model1}(\mathbf{Q})$ and $A_{model2}(\mathbf{Q})$. To determine $A_{Pb}(\mathbf{Q})$, we simply calculated it from the submonolayer coverage, determined by XSW, and the assumed adsorbate position z relative to the calcite surface. Finally, to determine which calcite layer contained the Pb submonolayer, we compared the intensity calculated using Eqn. 3 with the measured intensity for different assumed locations of the Pb submonolayer. As shown in detail in the results section, we find the same location of the Pb ions for both calcite models: >70% of the Pb ions are in the surface layer of the calcite crystal.

3. EXPERIMENTAL PROCEDURES

High-quality spar calcite from Brazil and dilute aqueous Pb-bearing solutions were used in our experiments. The calcite was cut into rectangular blocks that yielded cleavage faces having areas of 7 mm × 7 mm. Two experimental solutions were prepared by mixing 0.05 M $CaCl_2$, 0.10 M $NaHCO_3$, and deionized water in approximate proportions of 1:50:450. The pH of one solution was adjusted to 8.0 using 1 M HNO_3 and the pH of the other was adjusted to 9.0 using 0.1 M NH_4OH. To each of these solutions we added about 2 g of pre-washed calcite powder (90–125 micron particle size). To obtain calcite-saturated solutions, these mixtures were stirred using a magnetic stir bar and equilibrated with air for over 24 h, and then filtered using 0.45 μm polypropylene syringe filters. Aliquots of these calcite-saturated solutions were used without further treatment in the Pb free calcite X-ray reflectivity measurements. Finally, a solution with 1.0 mM Pb and 1.2 mM ethylenediaminetetraacetic acid (EDTA) concentrations, prepared from Pb nitrate and disodium EDTA salts, was mixed with the calcite-saturated filtrates in approximate proportions of 1:10. The EDTA was added to ensure undersaturation of Pb-bearing solid phases, so that the structure of adsorbed Pb on calcite could be studied without the deposition of other Pb-bearing phases. The initial compositions of the resulting experimental solutions are given in Table 1. The final compositions of the solutions were not measured. As determined by mass balance, however, the estimated change in total solution Pb concentration caused by adsorption onto calcite was only about 0.01% of the initial concentration. Table 2 shows the speciation of Pb in these solutions, calculated using the program MINTEQA2 (Allison et al., 1991) at 25 °C and atmospheric CO_2 pressure ($10^{-3.5}$ atm). The thirteen Pb-bearing solid phases in the database of MINTEQA2 (including cerrusite, cotunnite, phosgenite, massicot, litharge, laurionite, hydrocerrusite, hydrated Pb-oxide, Pb-hydroxychloride, and other Pb-hydroxides and Pb-oxycarbonates) were generally extremely undersaturated in our initial experimental solutions under these conditions. They had saturation indices ranging from −6 to −28 in solutions 1 and 2, and from −0.3 to −11.2 in solution 3. The saturation index is given by log IAP/K_{sp}, where IAP is the ion activity product and K_{sp} is the equilibrium solubility product constant. Calcite saturation indices were −6.6 and −6.4, respectively, for solutions 1 and 2, and −0.04 for solution 3.

For the X-ray measurements, the calcite was freshly cleaved and immediately submerged in 4 mL of an experimental solution in a loosely capped 7 mL Teflon vial. The partial pressure of CO_2 was not controlled other than by contact with atmosphere. Reaction times prior to X-ray measurements ranged from 4.3–38.5 h. Immediately prior to the X-ray measurements, most of the reacted solution was removed from the vial using a plastic pipet, leaving the calcite crystal with a mound of solution covering the cleavage surface. For the ex situ XSW measurements, the remaining solution was blown from the calcite surface with a jet of compressed nitrogen, and the sample was immediately placed in a flowing helium atmosphere for the duration of the measurements. No time dependent changes in the samples were noted during the ex situ XSW measurements. For the in situ XSW and reflectivity measurements, the calcite crystal was carefully placed in the X-ray cell using Teflon-coated tweezers (without touching the cleavage surface), and a 10–100 μm capillary layer of the solution was trapped between the calcite cleavage surface and a 12 μm polypropylene film.

The XSW measurements were performed at beamline X15A at the National Synchrotron Light Source (NSLS) using an incident X-ray energy of 13.8 keV. This beamline is described by Qian et al. (1994). Our previously described XSW technique (Qian et al., 1994) was used to triangulate the three-dimensional lattice location of adsorbed Pb at the calcite surface ex situ on one sample, using three separate Bragg reflections. We also measured the (104) reflection on three other crystals. For one of these crystals, we first made an in situ XSW measurement so we could directly compare the in situ Pb structure with that determined ex situ for the same surface. Coverages of Pb were determined by comparison of the off-Bragg Pb fluorescence intensity to that of a Pb-implanted Si standard having a Pb concentration of 1×10^{15} Pb atoms per cm^2. Unreacted calcite showed negligible Pb fluorescence. A 0.05 mm thick Al foil was placed before the fluorescence detector to attenuate the strong fluorescence from Ca.

The X-ray reflectivity measurements were performed at beamline X6B at the NSLS using an incident X-ray energy of 9.0 keV. A more detailed description of this beamline is given by Chiarello and Sturchio (1995). We performed several in situ X-ray reflectivity measurements of calcite-water and calcite-Pb-water interfaces using the method described by Chiarello and Sturchio (1995). Each reflectivity measurement was performed using a new (104) cleavage of the same calcite crystal, and the calcite-Pb-water measurements used aliquots of solution 1 (Table 1). Seven calcite-water interfaces without Pb and two calcite-Pb-water interfaces were measured. All

Table 2. Pb speciation in solution[a].

	Solution 1	Solution 2	Solution 3
Pb^{2+}	−16.2	−16.3	−8.52
$PbCl^+$	−17.9	−18.4	−10.6
$PbCl_2^0$	−21.0	−21.8	−14.2
$PbCl_3^-$	−24.4	−25.6	−18.0
$PbCl_4^{2-}$	−28.1	−29.5	−22.0
$Pb(CO_3)_2^{2-}$	−13.7	−12.5	−8.47
$PbOH^+$	−15.1	−14.9	−8.05
$Pb(OH)_2^0$	−15.7	−15.2	−9.28
$Pb(OH)_3^-$	−17.9	−17.0	−12.0
$Pb_2(OH)^{3+}$	−29.9	−29.9	−15.2
$Pb_3(OH)_4^{2-}$	−37.3	−36.3	−16.7
$PbCO_3^0$	−13.0	−12.5	−6.57
$Pb(OH)_4^{2-}$	−20.7	−19.6	−15.5
$PbHCO_3^+$	−15.8	−15.7	−8.79
$PbEDTA^{2-}$	−4.26	−4.14	−5.12
$PbHEDTA^-$	−21.2	−21.5	−21.5
PbH_2EDTA^0	−33.5	−34.0	−33.1

[a] log activity at 25°C and $10^{-3.5}$ atm CO_2

Table 3. Results of X-ray standing wave measurements.

Sample	Time[a]	Solution[b]	Experiment	P_H	f_H	Θ_t[c]	Θ_c[d]
A[e]	5.3	1	(104) ex situ	0.00	0.59	0.08	0.05
			(006) ex situ	0.52	0.64	0.08	0.05
			(024) ex situ	−0.01	0.63	0.08	0.05
B[f]	7.5	2	(104) in situ	−0.01	0.48	0.08	0.04
			(104) ex situ	−0.01	0.55	0.08	0.05
C	38.5	2	(104) ex situ	0.01	0.74	0.10	0.07
D	12.5	2	(104) ex situ	0.00	0.48	0.05	0.02
E[g]	8.0	3	(104) ex situ	0.00	0.66	0.08	0.05

[a] reaction time in hours
[b] solution compositions given in Table 1
[c] Θ_t is total coverage in monolayers (ML). One ML is 5.0×10^{14} atoms/cm^2
[d] Θ_c is the coherent coverage given by $\Theta_c = f_H \times \Theta_t$
[e] data for sample A shown in Fig. 3
[f] data for sample B shown in Fig. 4
[g] data for sample E shown in Fig. 3 of Qian et al. (1994)

measurements were performed in the specular geometry, with the wavevector transfer **Q** perpendicular to the (104) plane.

The AFM measurements were conducted at room temperature using a commercial AFM capable of operating in solution environments (Nanoscope III, Digital Instruments, CA). Fresh cleavage surfaces of the same calcite used in the X-ray experiments, and a Pb-bearing solution composition similar to that of solutions 1 and 2 (Table 1), were used. The solution cell was made of glass and sealed with a pliable O-ring placed between the sample and the cell. The volume of the solution cell was approximately 20 μL with an exposed sample surface area of 28 mm^2. The solution was injected into the cell through a syringe filter. Commercial Si_3N_4 cantilevers with a spring constant of 0.12 N/m were used for imaging. The calcite samples typically had a rhombohedral shape, about 10 mm x 10 mm in area and 1–2 mm thick. The surfaces were prepared by cleaving the crystal along the (104) cleavage plane in air with a clean razor blade. Detailed experimental procedures are described by Liang et al. (1996).

4. RESULTS

This section describes the results of our XSW, X-ray reflectivity, and AFM measurements. It also explains how parts of our X-ray reflectivity models were inspired by the AFM measurements, and how our reflectivity models were constructed so they could include the constraints imposed by the XSW and AFM results.

4.1. X-Ray Standing Wave Measurements

Table 3 summarizes the results of our XSW measurements for four calcite samples, along with the ex situ results from Qian et al. (1994), shown for comparison. From the XSW measurements, values for the coherent position P_H and the coherent fraction f_H of Pb were derived by fitting the Pb fluorescence yield as a function of angle according to Eqn. 1. The total Pb coverage was measured from the off-Bragg Pb fluorescence intensity. The values of the coherent position P_H for all tabulated XSW measurements for the (104) Bragg reflection have a mean and standard deviation of 0.00 ± 0.01. This indicates that the sorbed Pb ions occupy positions in the (104) lattice plane, with a 1σ experimental error of about ±0.03 Å. To determine the in-plane position of Pb ions within the (104) plane, ex situ XSW measurements for sample A were also made using two other reflections, (006) and (024). The XSW results for this triangulation experiment on sample A are shown in Fig. 3. The respective Bragg diffraction planes in the calcite lattice are shown in the insets of Fig. 3. The coherent position P_H for the (006) reflection was 0.52 ± 0.02 and that for the (024) reflection was −0.01 ± 0.02. These data are consistent with the Pb ions occupying the Ca sites in the calcite lattice, within the experimental errors of ±0.06 Å along the (006) direction and ±0.04 Å along the (024) direction.

The coherent fraction f_H values for all the XSW measurements in Table 3 range from 0.48–0.74, with a mean and standard deviation of 0.60 ± 0.09. Thus about 60% of the sorbed Pb occurs in the Ca sites in the calcite lattice, and about 40% of the sorbed Pb is not well ordered. We will refer to these fractions as the ordered coverage and the disordered coverage, respectively. The total Pb coverage calculated from off-Bragg fluorescence for all samples had a mean and standard deviation of 0.08 ± 0.02 equivalent monolayers (ML). One equivalent monolayer contains 5×10^{14} atoms/cm^2, for the Ca sites in the calcite (104) lattice plane. The ordered Pb coverage (which is very well approximated as the product of total coverage and coherent fraction) ranged from 0.02–0.07 ML and had a mean and standard deviation of 0.05 ± 0.02 ML. The incoherent fraction (total coverage minus ordered coverage) was consistently 0.03 ML. The XSW data are not sensitive to the location of the disordered Pb coverage because it is randomly distributed on the length scale of the calcite lattice d-spacing.

Comparisons between the in situ and ex situ measurements on sample B are shown in Fig. 4. These data indicate that neither the coherent position relative to the (104) planes nor the coherent fraction changed significantly when the conditions were changed from in situ to ex situ.

The P_H and f_H values, as well as the total Pb coverages, for all of the samples in Table 3, have small ranges and do not exhibit dependence on time, pH, or the activities of aqueous Pb species, within the range of conditions studied. This indicates that: (1) the observed coverages may represent saturation of the available adsorption sites at the calcite surface and (2) the adsorption is surface-controlled.

4.2. Specular X-Ray Reflectivity Measurements

Because the specular X-ray reflectivity depends on the interference between the reflection from the Pb ions and the

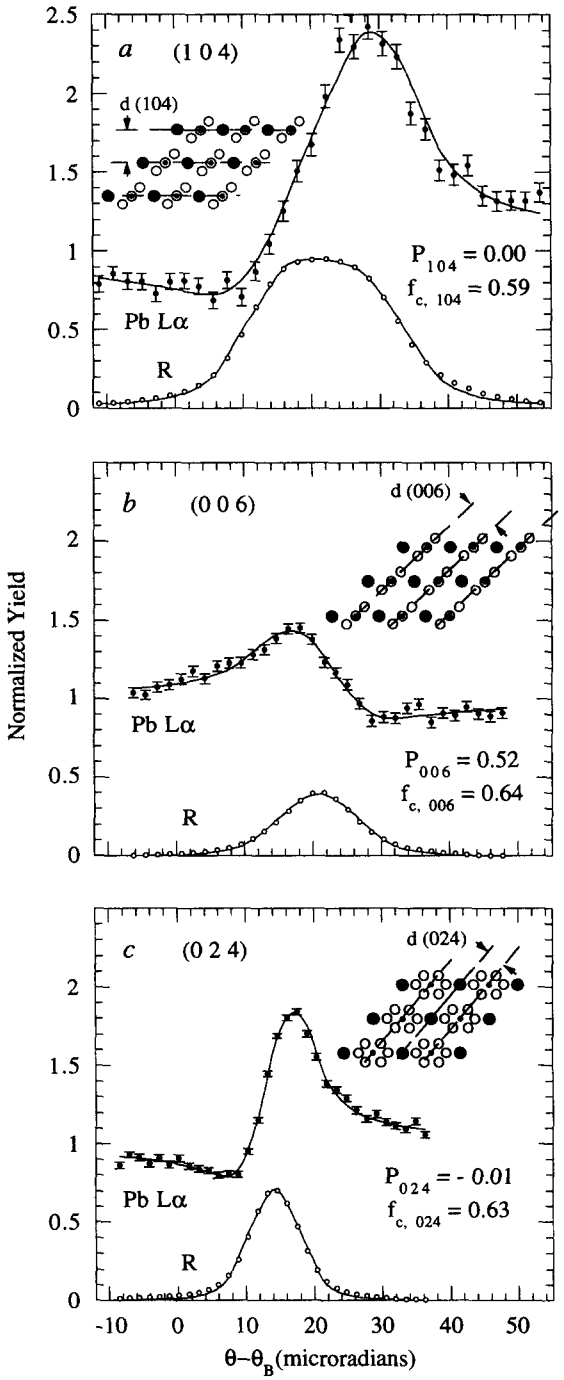

Fig. 3. Normalized Pb Lα X-ray fluorescence yield and reflectivity (R) vs. incidence angle for the ex situ XSW measurements performed on calcite sample A. Data for three different Bragg reflections are shown: (a) 104, (b) 006, and (c) 024. The structures of these diffraction planes are shown in the insets, where the Ca, C, and O atoms are represented by shaded, solid, and open circles, respectively. Solid lines are the best fits to the Pb fluorescence yield $Y(\theta)$ data. Using Eqn. 1, we obtained the values of P_H and f_H shown in the figure from these fits. In all three cases, the coherent position P_H indicates that Pb occupies the Ca site with a high coherent fraction $f_H \cong 0.6$. Note that the (006) diffraction planes coincide with the carbonate planes. Therefore, in this measurement, $P_H = 0.5$ for the Ca position.

reflection from the calcite-water interface, it is extremely sensitive to the precise location of the Pb ions near the surface. The XSW measurements show that the coherent fraction of the Pb ions occupies Ca sites in the calcite lattice, but the XSW measurements cannot determine the specific layer of calcite which contains the Pb ions. Since we only need to determine which layer the Pb ions occupy, the measured in situ specular X-ray reflectivity for calcite (with and without Pb) can be used. In this section, we show how the reflectivity measurements establish that the Pb submonolayer goes primarily into the surface layer of calcite. This conclusion is independent of the exact morphology of the calcite surface. In fact, the exact structure of the calcite surface is still an unsolved problem that we are in the process of solving by combining surface X-ray crystallography and AFM.

We can determine the location of the Pb ions because the interference between the reflection amplitudes for the Pb submonolayer and the calcite-water interface is so sensitive to the precise location of the Pb. It is also important that the phase of the reflected amplitude from the calcite-water interface is rather insensitive to the exact structure of this interface. The magnitude of the reflection amplitude for the calcite-water interface, but not the phase, can be directly determined from the measured reflectivity. To determine the phase we made many models of the calcite-water and calcite-Pb-water interfaces. Within the range of models consistent with our specular reflectivity data and our AFM measurements, the interference between the calcite-water amplitude $A_{calcite}$ (Q) and the Pb amplitude A_{Pb} (Q) is almost independent of the calcite-water interface model. This allows us to establish the location of the Pb submonolayer independently of the exact structure of the calcite-water interface.

Possible locations of the adsorbed Pb ions near the calcite-water interface are shown schematically in Fig. 5. The num-

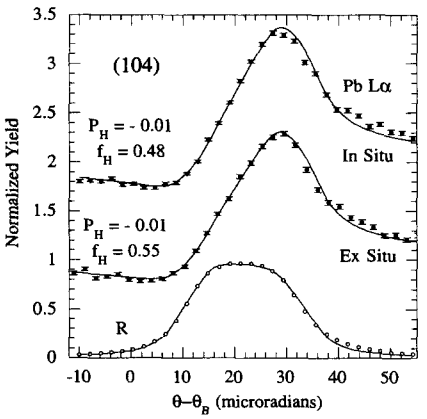

Fig. 4. Normalized Pb Lα X-ray fluorescence yield and reflectivity (R) vs. incidence angle for in situ and ex situ XSW measurements performed on calcite sample B. The solid lines are the best fits to the Pb fluorescence yield $Y(\theta)$ data. Using Eqn. 1, the values of P_H and f_H shown in the figure were derived from these fits. Note that the coherent positions P_H determined from in situ and ex situ measurements are identical, indicating no significant difference in the position of the adsorbed Pb atoms. The coherent fraction f_H is slightly smaller for the in situ measurement because of randomly distributed Pb in the solution layer.

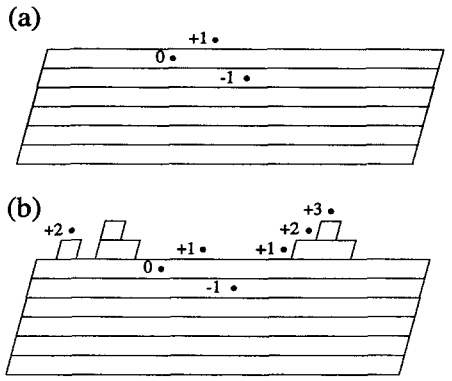

Fig. 5. Schematic diagram showing the possible locations of the Pb ions adsorbed on (a) smooth and (b) rough calcite surfaces. Pb ion positions are labeled by calcite (104) layer position with respect to the surface. The surface layer is designated as the 0 layer position.

ber of these locations depends on the morphology of the calcite-water interface. In the limit of smooth calcite, having a very low step density, shown in Fig. 5a, the most likely locations for the Pb ions are: (a) in the surface layer, designated layer 0; (b) one layer below the surface, designated layer -1; and (c) one layer above the surface, designated layer $+1$. In the limit of a calcite surface with two partial layers, shown schematically in Fig. 5b, the most likely locations for the lead are: (a) in the surface layer, designated layer 0; (b) one layer below the surface, designated layer -1; (c) one layer above the surface, designated layer $+1$; (d) two layers above the surface, designated layer $+2$; and (e) three layers above the surface, designated layer $+3$. There are actually three structurally inequivalent kinds of $+1$ and $+2$ sites; the adsorbed Pb ions can be in the middle of a terrace, at a step edge with an obtuse angle, or at a step edge with an acute angle. However, the specular X-ray reflectivity cannot distinguish between these structurally inequivalent $+1$ and $+2$ sites.

The calculated calcite specular reflectivity for different locations of the 0.05 ML Pb submonolayer is shown in Fig. 6. This calculation assumed that the calcite was ideally terminated, but the changes shown in this figure for ideally terminated calcite are very similar to the changes produced for more realistic calcite-water interface models that agree with the measured specular reflectivity in more detail. When the Pb submonolayer occupies the calcite surface layer, the intensity of all the midzones are increased relative to the intensity of the midzones without Pb. If the Pb submonolayer goes into any other layer, however, the intensity produced by adding the Pb produces both oscillations in the intensity and regions where the intensity is lower than it is without the Pb. It is the clear increase in the midzone intensities and the absence of the predicted midzone oscillations in the measured calcite-Pb-water reflectivity that demonstrates the Pb submonolayer goes primarily into the surface layer of the calcite.

Our measured specular reflectivity shows that the calcite-water interface is not ideally truncated because the middle of the second and third Brillouin zones have clear structure. The best fit to the data for ideally truncated calcite (with and without Pb) is shown in Fig. 7a. Note that the observed increase in the intensity of the middle of the first, second, and third Brillouin zones is very similar to the increase calculated for the ideally truncated model, but that this model does not provide a reasonable fit to the data. What causes the observed midzone structure? The three most likely sources of this midzone structure are (1) surface reconstruction, (2) surface relaxation, and (3) partial layers on the surface. We have constructed many models of the calcite surface with these three ingredients, and we have been able to produce satisfactory fits to the measured reflectivity data using two of these models (see Fig. 7b and c). The details of these models are beyond the scope of this paper but the important aspects of these models for the current study are as follows. (1) We can fit the calcite reflectivity data with a model where the surface is smooth and we vary only the positions of the oxygen atoms in the two surface layers (i.e., we vary the positions of the oxygen atoms in layer 0 and layer -1). The quality of the fit is shown in Fig. 7b. This model was motivated by the atomic resolution AFM data of Liang et al. (1996) that indicate relaxation of the oxygen atoms within the surface unit cell. We will refer to this model as the oxygen relaxation model. (2) We can also fit the calcite reflectivity data with a model that includes partial layers. The quality of the fit is shown in Fig. 7c. This model was motivated by the topographic AFM data presented in the next section. However, the addition of the partial layers alone does not produce an adequate fit. We must still include some oxygen relaxation of the partial layers and the top calcite layer to obtain the fit shown. We will refer to this model as the partial layer model. Both best-fit models for the X-ray reflectivity data require significant (0.1–0.3 Å) relaxations of oxygen atoms in the uppermost layers of calcite. These relaxations are consistent with the sizes of the oxygen relaxations suggested by the atomic resolution AFM measurements of Liang et al. (1996).

Although we must introduce a modification of the surface

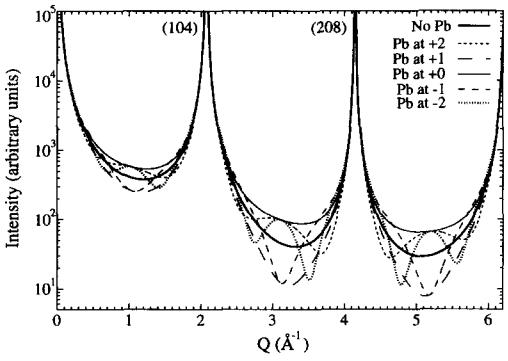

Fig. 6. The calculated changes in the specular CTR intensity for ideally truncated calcite produced by adding 5% of a Pb monolayer in the Ca sites in different layers. When the Pb goes into the surface layer (layer 0), the midzone reflectivity increases smoothly in the first, second, and third Brillouin zones. Note that for all the other Ca sites (viz., layers -2, -1, $+1$, $+2$) the midzone reflectivity develops oscillatory midzone structure. The absence of this oscillatory midzone structure proves that most (>70%) of the Pb must go into the surface layer (i.e., into layer 0).

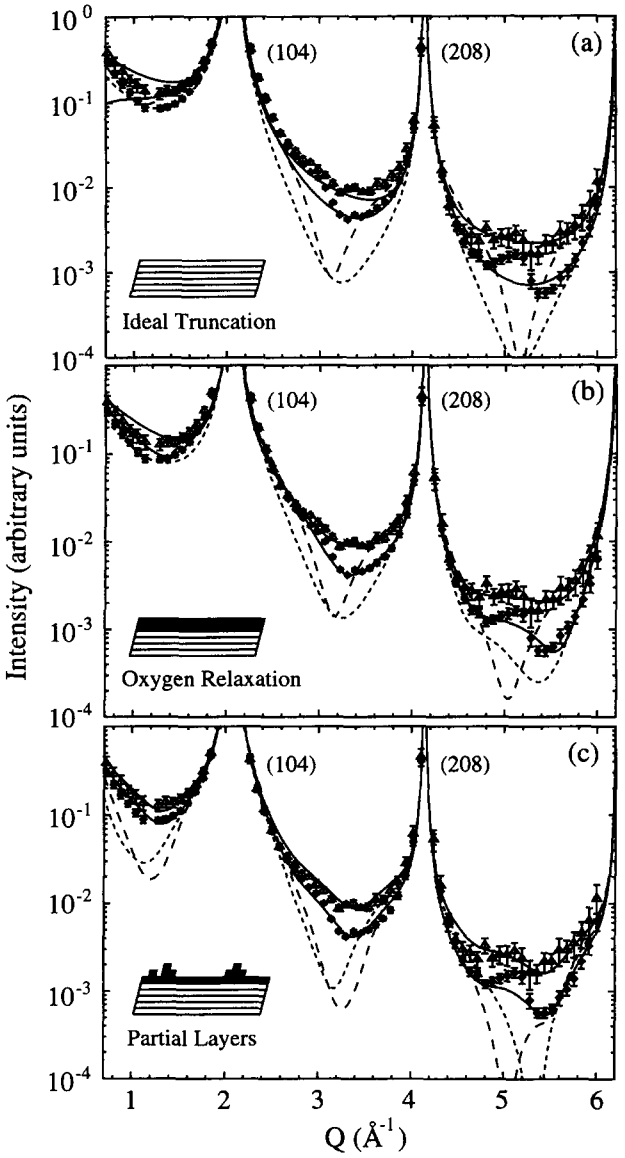

Fig. 7. Comparison of the measured and calculated in situ X-ray reflectivity intensities from calcite with and without adsorbed Pb. Solid lines are best fits to the measured reflectivity intensities from the calcite-water interface with Pb (triangles) and without Pb (diamonds). Calculations are shown for three different models of the calcite surface: (a) ideally truncated calcite, (b) smooth (ideally truncated) calcite with oxygen relaxation in the top two calcite layers, and (c) rough (two partially occupied layers above the surface layer) calcite with oxygen relaxation in the top calcite layer and in the two partial layers. Note that the measured midzone reflectivity increases when the Pb is adsorbed. This agrees with the reflectivity change calculated for Pb atoms going into the Ca sites in the surface layer (top solid line) and disagrees with the changes calculated for Pb atoms going into Ca sites one lattice spacing above (dashed line) or below (dotted line) the surface.

structure of calcite to model the midzone structure observed in the measured X-ray reflectivity, this structure does not appreciably change the phase of the calcite reflectivity. This is the reason that the interference between the Pb reflectivity and the calcite reflectivity looks qualitatively the same for ideally-terminated calcite (no oxygen relaxation), smooth calcite with oxygen relaxation, and rough calcite (with partial layers and oxygen relaxation). Since the measured X-ray reflectivity has features near the middle of the second and third Brillouin zones, the simplest models that will produce features here will have a surface layer which is twice as large in real space as the d-spacing of the (104) lattice planes. Both our two partial layer model and our oxygen relaxation model have strong features which are twice as wide as the (104) d-spacing.

How well can we determine the exact location of the Pb submonolayer? From the fits shown in Fig. 7b and 7c, we can see that if all of the Pb is put into the same layer, then only Pb in the surface layer is consistent with the measured reflectivity. If all of the Pb is put into any layer except the surface layer, the measured reflectivity would have large midzone features which are not observed. However, it must still be possible to put a small amount of the Pb into layers above or below the surface layer and still agree with the measured reflectivity. We investigated this to see how sensitive our X-ray reflectivity data is to the exact location of the Pb submonolayer. To calculate our sensitivity, we kept the total amount of Pb fixed at 0.05 ML and split this total between the surface layer and one of the alternative layers in 0.002 ML steps. For each possible layer, we calculated the reflectivity that would be produced if the Pb ions were distributed $(1 - x)$ in the surface layer and x in one of the other layers. For each case, we found that at least 70% of the total (i.e., 0.035 ML) had to be in the surface layer, but that up to 30% of the total (i.e., 0.015 ML) could be in one of the alternative layers. In the special case where 70% is in the surface layer (in layer 0) and 30% is in the partial layer one layer up (in layer +1), then essentially 100% of the ordered Pb ions are in the Ca sites directly exposed to the solution.

We have assumed throughout this analysis that the disordered Pb does not contribute to the X-ray reflectivity. This is a reasonable assumption because the disordered Pb must be distributed randomly on the length scale of the calcite lattice d-spacings in order to be consistent with the XSW results. We verified with model calculations that 0.03 ML of Pb distributed randomly over 4 Å would not contribute to the measured X-ray reflectivity.

4.3. Atomic Force Microscopy Measurements

There have been numerous in situ AFM studies of calcite-water interfaces (e.g., Hillner et al., 1992; Gratz et al., 1993; Ohnesorge and Binnig, 1993; Dove and Hochella, 1993; Stipp et al., 1994; Liang et al., 1996), but we found no published AFM studies of the surface of calcite with adsorbed Pb. AFM images of the calcite surface used in our X-ray experiments under our experimental conditions are shown in Fig. 8. The surface of calcite appears similar under the two experimental conditions, i.e., the topography for calcite in Pb-free, calcite-saturated solution, shown in Fig. 8a, and the topography for calcite in the Pb-EDTA solution, shown in Fig. 8b, are very similar. In both cases, there is a low step density and there are a few partial layers on the surface. These AFM results show qualitatively that the two

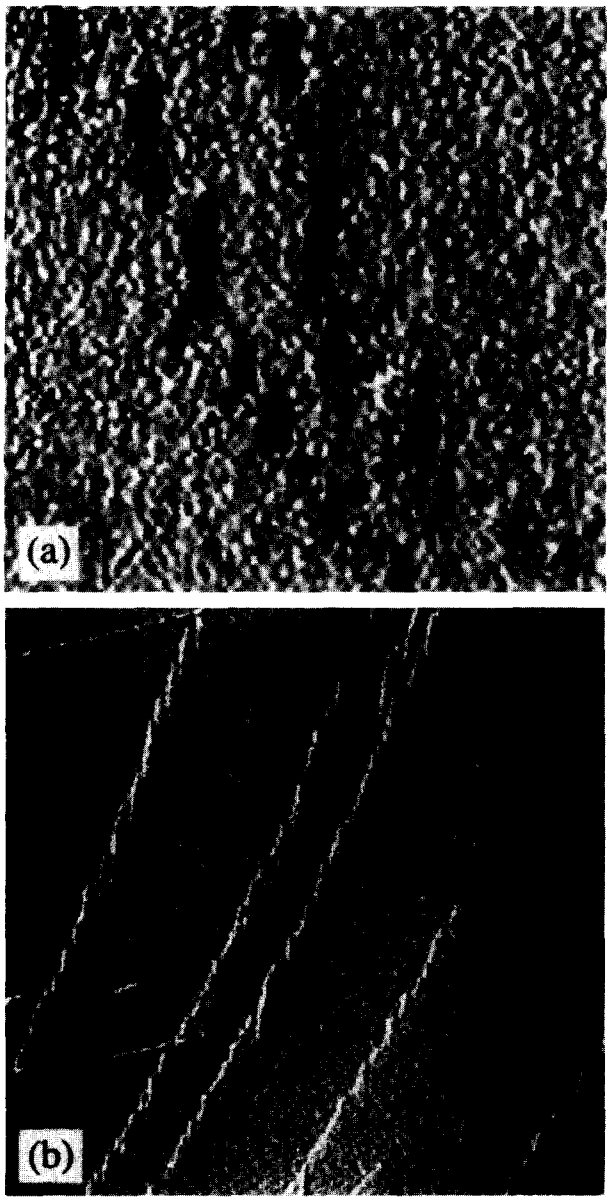

Fig. 8. Variable deflection AFM images of calcite, from a portion of the same crystal used in the X-ray experiments. (a) Image of (104) cleavage surface following reaction with deionized water for 3.5 h. (b) Image of (104) cleavage surface following reaction for 2 h with 100 μM Pb-EDTA solution similar to the Pb-bearing solutions used in the X-ray experiments. Both images are of 2 × 2 μm areas and exhibit similar step densities.

partial layer X-ray reflectivity model presented in the previous section is physically reasonable.

To make a more quantitative comparison between the morphology of the AFM images and the morphology derived from the X-ray reflectivity models, we need to know how the X-ray photons sample the calcite surface. If the photon coherence area projected onto the calcite surface was exactly the size of the images shown (i.e., if the coherence area was 2 μm × 2 μm) then the number of partial layers that would be sampled by the photons would be equal to the number of partial layers visible in the figure. In Fig. 8a, two partial layers are visible, and in Fig. 8b, six partial layers are visible. However, we do not think this difference is necessarily significant because of our very limited sampling of all possible surface configurations. In addition, when we sample these two images using the photon coherence area (4 μm × 400 Å) that we calculate using the beamline characteristics, we find that the results for these two images are remarkably similar. In this case we find that the photons will see two partial layers for the calcite surface without Pb (Fig. 8a) and three partial layers for the calcite surface with Pb (Fig. 8b). Many more AFM images must be analyzed to accurately determine the ensemble average morphology with and without Pb. However, the simple analysis presented above already shows that the AFM images and the X-ray reflectivity measurements produce remarkably similar views of the morphology of the calcite surface.

5. DISCUSSION

The XSW measurements show that there are 0.05 ML of ordered Pb in Ca sites and 0.03 ML of disordered Pb. The X-ray reflectivity measurements show that most (>70%) of the ordered Pb goes into the calcite surface layer. However, neither the XSW technique nor the X-ray reflectivity technique can provide any information about the location of the disordered Pb. In this section, we first discuss the thermodynamics and the microscopic energetics of the ordered Pb. Why does the Pb go into Ca sites even though the divalent Pb ions are 20% larger than the divalent Ca ions that they are replacing? And why does the Pb go into the surface layer rather than to the step edges, the terrace sites, or the bulk sites? Then we discuss the possible speciation and distribution of the disordered Pb coverage.

5.1. Thermodynamics and Microscopic Energetics of the Ordered Lead

The incorporation of Pb in bulk calcite is prohibited by the large ionic radius of divalent Pb (1.20 Å) relative to that of Ca (0.99 Å) (Reeder, 1983). Although seemingly paradoxical, there are good thermodynamic arguments indicating that calcite should have a high affinity for Pb. A linear correlation exists between the standard Gibbs free energies of formation of rhombohedral carbonates and the standard Gibbs free energies of their aqueous divalent cations (Sverjensky, 1984; Sverjensky and Molling, 1992). This correlation allows prediction of the thermodynamic equilibrium constant for the distribution of divalent cations between calcite and aqueous solution. For our case, this equilibrium constant is proportional to the difference in free energy between the aqueous Pb^{2+} and Ca^{2+} ions. This free energy relationship predicts a relatively large value of the distribution coefficient $D_{Pb,calcite}$ that can be evaluated experimentally for Pb between calcite and solution,

$$D_{Pb,calcite} = (X_{Pb}/X_{Ca})_{calcite}\,(a\mathrm{Ca}^{2+}/a\mathrm{Pb}^{2+})_{aqueous} \quad (4)$$

where X is the solid mole fraction and a is the aqueous activity. A $D_{Pb,calcite}$ value close to that for Cd and Zn should

be expected according to Fig. 2a of Sverjensky and Molling (1992).

The thermodynamic equilibrium constant for Pb distribution between calcite and aqueous solution can also be approximated by the ratio of the equilibrium solubility product constants K_{sp} for calcite and cerrusite,

$$K_{Pb,calcite} = (K_{sp}CaCO_3)/(K_{sp}PbCO_3) \quad (5)$$

assuming an ideal solid-solution. Thus, with log K_{sp} values of −8.48 for calcite and −12.9 for cerrusite, a log $K_{Pb,calcite}$ value of 4.4 is predicted. In the case of an ideal solid solution, $D_{Pb,calcite}$ from Eqn. 4 and $K_{Pb,calcite}$ from Eqn. 5 would be equal. The experimental values obtained in this study for log $D_{Pb,calcite}$, by using the calculated equilibrium speciation of the initial solutions and the mean value of 0.05 for the solid mole fraction ratio, $(X_{Pb}/X_{Ca})_{calcite}$, are 3.6 for solution 1, 3.9 for solution 2, and 4.0 for solution 3. In comparison, some experimentally determined values for log $D_{Cd,calcite}$ are 3.2 (Davis et al., 1987) and 3.0 (Zachara et al., 1991). The significant discrepancy between our $D_{Pb,calcite}$ values and that predicted using Eqn. 5, 4.4, may indicate nonideal solid-solution behavior for Pb in the surface layer of calcite. The thermodynamic driving force for Pb incorporation into calcite appears to account for the significant incorporation of Pb in the surface layer of calcite that we observe.

What are the microscopic energetics that determine where the Pb atoms will go? Which of the adsorption sites shown in Fig. 5 will have the lowest free energy? Will they sit on top of a terrace surrounded by their hydration shell? Will they sit at step edges? Will they go into the Ca sites in the surface layers exposed to the solution? Or will they go into Ca sites below the surface?

If the Pb ions were the same size as the Ca ions, the lowest energy site would be one of the Ca sites inside the crystal. Of course, the Pb ions would still need to diffuse into the crystal from the surface and this would limit their incorporation into bulk sites. However, since the Pb ions are 20% larger than the Ca ions, the Pb is too large to fit into the bulk Ca sites. We find that the Pb ions go into the surface layer. This implies that the decrease in the Coulomb energy obtained by going into the surface layer must be larger than the repulsion caused by the Pb ion being too large to fit into the Ca site. We argue that it is not obvious a priori whether the Pb ions would prefer to go into the Ca sites in the surface layer or to go to step edges. When a Pb ion goes to a step edge it can reduce its Coulomb energy by interacting with the carbonate ions and it doesn't have to pay the repulsive energy cost due to its larger ionic radius that it must pay to go into a surface Ca site; its Coulomb energy is also reduced by the partial hydration shell that will surround it away from the step edge. However, our X-ray measurements show that the Pb ions go into the Ca surface sites, and our AFM measurements show that our samples have an insufficient length of step edge to accommodate all the Pb ions observed on the surface. Placing Pb ions as densely as possible (i.e., one Pb ion every 3 Å) along the entire step edge shown in Fig. 8b corresponds to a Pb coverage of 0.0006 mL, almost one hundred times less than the observed ordered Pb.

Another possible location of the Pb ions is just above the surface, in the middle of one of the terraces. In this case, there is no additional repulsion due to the size of the Pb ions, and there is some reduction of the Coulomb energy of the Pb due to its interaction with the surface carbonate ions and with its hydration shell. However, since the Coulomb reduction due to the hydration shell is probably much less than the reduction due to the interaction with the surface, it seems likely to us that this case will have a higher energy than the surface sites and the step edges. The balance between the lattice Coulomb energies, the oversize repulsive energy, the hydration energy, and additional energies of comparable importance must be considered. The Madelung problem for the possible sites shown in Fig. 5 is clearly of great relevance to this problem.

5.2. Origin of the Disordered Lead Coverage

We noted above that the disordered Pb coverage has a random distribution and, therefore, probably comes from Pb ions which are distributed in z. This distribution might arise from physisorbed hydrated Pb ions or complexes, or from a mixture of chemisorbed Pb species that is effectively random. These Pb ions or complexes may be adsorbed at the calcite surface or associated with surface contaminants. What species are viable candidates for the 0.03 equivalent monolayer coverage of disordered Pb that we observe?

First, we consider Pb-EDTA^{2-}, which was the most abundant Pb species in our experimental solutions, being orders of magnitude more abundant than any other Pb species (see Table 2). Bowers and Huang (1986) showed that divalent metal-EDTA complexes including Cd, Cu, Ni, Pb, and Zn all exhibit the same ligand-like, pH-dependent, and metal independent adsorption behavior on γ-Al_2O_3; they interpreted this in terms of hydrogen bonding between metal-EDTA molecules and $AlOH_2^+$ surface sites. Similar behavior of divalent metal-EDTA complexes was observed for adsorption onto goethite (Nowack and Sigg, 1996). Davis et al. (1987) used EDTA in their experiments on Cd sorption by calcite in calcite-saturated solutions of low ionic strength at pH values of 6.5–8.0. Using ^{14}C-labelled EDTA they detected no adsorption of EDTA under these conditions. By analogy, assuming similar behavior of the Pb-EDTA and Cd-EDTA complexes in this system, we would expect no Pb-EDTA adsorption to have occurred under our experimental conditions that involved somewhat higher pH values (8.78–9.11), and concomitantly lower surface charge values, than the experiments of Davis et al. (1987). Thus, we argue that the disordered Pb coverage cannot be attributed to the adsorption of Pb-EDTA.

After Pb-EDTA, the next most abundant aqueous Pb species are (in order of decreasing abundance) $PbCO_3°$, $Pb(CO_3)^{2-}$, $PbOH^+$, $Pb(OH)_2°$, $PbHCO_3^+$, and Pb^{2+}. Our X-ray data indicate that Pb^{2+} exchanges for Ca^{2+} in the calcite surface layer. Although some or all of these aqueous Pb species could be involved in such a surface ion-exchange reaction, the X-ray data of this study do not constrain the detailed mechanism of this reaction. It is possible that some of these species could be adsorbed at other sites above the calcite surface layer.

Another possibility that must be considered is that the disordered Pb is associated with adventitious hydrocarbon

contamination that may have resulted from the brief exposure of the sample surface to the laboratory atmosphere. The amount of this type of contamination found on differently prepared calcite surfaces, and its effect upon XPS and LEED measurements on calcite, were studied by Stipp and Hochella (1991). If adventitious material contaminated the calcite surface in our experiments, and it had a random spatial distribution, then any Pb associated with it would also have had a random spatial distribution that would be consistent with the XSW results.

Previous studies have pointed out the importance of surface defects (including step edges, kinks, dislocations, impurities, and vacancies) in controlling the location of adsorbates (see, e.g., the reviews by Hochella, 1990, 1995). However, the AFM images acquired for this study (see Fig. 8) show a very low step density, on the order of one step per μm of surface length. As shown above, this step density is far too low to account for the observed coverage of Pb. No other obvious surface defects were observed in the AFM images.

6. CONCLUSIONS

The location of Pb ions adsorbed at the calcite (104)-water interface from dilute aqueous solutions was investigated in situ using synchrotron X-ray standing wave and X-ray reflectivity techniques. The X-ray standing wave measurements indicated that there was a total of 0.08 equivalent monolayers of adsorbed Pb at the interface, that 60% of the adsorbed Pb occupied Ca sites in the calcite lattice, and that 40% of the adsorbed Pb was disordered. The X-ray reflectivity measurements indicated that the ordered Pb occupying the Ca sites in the calcite lattice was mainly (>70%) in the surface atomic layer. This conclusion is independent of the exact model used to fit the calcite reflectivity data. The best fitting models for the X-ray reflectivity data involve relaxation of the oxygens near the calcite surface by a few tenths of an angstrom. Relaxations of this size are consistent with the oxygen relaxations suggested by the atomic resolution AFM images of Liang et al. (1996). Our AFM studies of the calcite (104) surface under experimental conditions similar to those of our X-ray experiments showed low step densities for calcite equilibrated with deionized water and with Pb-bearing solution. The measured step densities from our AFM images were consistent with those assumed for our X-ray reflectivity models. The combination of X-ray standing wave and X-ray reflectivity measurements, demonstrated here for Pb on calcite, has great potential for future studies of adsorption at mineral-water interfaces.

Acknowledgments—This work is supported by the Office of Basic Energy Sciences, U.S. Department of Energy under contracts W-31-109-Eng-38 to Argonne National Laboratory, DE-AC02-76CH00016 to the National Synchrotron Light Source/Brookhaven National Laboratory, and DE-ACO6-76RLO1830 to Pacific Northwest National Laboratory. Two anonymous reviewers gave constructive criticism that led to significant improvements in this manuscript.

Editorial handling: J. D. Macdougall

REFERENCES

Allison J. D., Brown D. S., and Novo-Gradac K. J. (1991) MINTEQA2/PRODEFA2, A Geochemical Assessment Model for Environmental Systems: Version 3.0 User's Manual. EPA/600/3-91/021. US EPA.

Als-Nielsen J. (1991) X-ray reflectivity studies of liquid surfaces. In *Handbook of Synchrotron Radiation,* Vol. 3 (ed. G. S. Brown and D. E. Moncton), pp. 471–503. North-Holland.

Andrews S. R. and Cowley R. A. (1985). Scattering of X-rays from crystal surfaces. *J. Phys. C: Solid State Physics* **18,** 6427–6439.

Batterman B. W. (1969) Detection of foreign atoms by their X-ray fluorescence scattering. *Phys. Rev. Lett.* **22,** 703–705.

Batterman B. W. and Cole H. (1964) Dynamical diffraction of X-rays by perfect crystals. *Rev. Mod. Phys.* **36,** 681–717.

Bedzyk M. J. and Materlik G. (1985) X-ray standing wave analysis for Br on Ge. *Surface Sci.* **152,** 10–16.

Bedzyk M. J., Bilderback D., Bommarito G. M., Caffrey M., and Schildkraut J. S. (1988) X-ray standing waves: A molecular yardstick for biological membranes. *Science* **241,** 1788.

Bedzyk M. J., Bommarito G. M., Caffrey M., and Penner T. L. (1990) Diffuse-double layer at a membrane-aqueous interface measured with X-ray standing waves. *Science* **248,** 52–56.

Bowers A. R. and Huang C. P. (1986) Adsorption characteristics of metal-EDTA complexes onto hydrous oxides. *J. Colloid Interface Sci.* **110,** 575–590.

Brown G. E., Jr., Parks G. A., and O'Day P. A. (1995) Sorption at mineral-water interfaces: macroscopic and microscopic perspectives. In *Mineral Surfaces* (ed. D. J. Vaughan and R. A. D. Pattrick), pp. 129–183. Chapman and Hall.

Chiarello R. P. and Sturchio N. C. (1994) Epitaxial growth of otavite on calcite observed in situ by synchrotron X-ray scattering. *Geochim. Cosmochim. Acta* **59,** 4557–4561.

Chiarello R. P. and Sturchio N. C. (1995) The calcite (104) cleavage surface in water: Early results of a crystal truncation rod study. *Geochim. Cosmochim. Acta* **59,** 4557–4561.

Chiarello R. P., Wogelius R. A., and Sturchio N. C. (1993) In situ synchrotron X-ray reflectivity measurements at the calcite-water interface. *Geochim. Cosmochim. Acta* **57,** 4103–4110.

Chisholm-Brause C. J., Hayes K. F., Roe A. L., Brown G. E., Jr., Parks G. A., and Leckie J. (1990) Spectroscopic investigation of Pb(II) complexes at the γ-Al_2O_3/water interface. *Geochim. Cosmochim. Acta* **54,** 1897–1909.

Cowan P. L., Golovchenko J. A., and Robbins M. F. (1980) X-ray standing waves at crystal surfaces. *Phys. Rev. Lett.* **44,** 1680–1683.

Davis J. A. and Kent D. B. (1990) Surface complexation modeling in aqueous geochemistry. In *Mineral-Water Interface Geochemistry* (ed. M. F. Hochella Jr. and A. F. White); *Rev. Mineral.* **23,** 177–305.

Davis J. A., Fuller C. C., and Cook A. D. (1987) A model for trace element sorption processes at the calcite surface: Adsorption of Cd^{2+} and subsequent solid-solution formation. *Geochim. Cosmochim. Acta* **51,** 1477–1490.

Dove P. M. and Hochella M. F., Jr. (1993) Calcite precipitation mechanisms and inhibition by orthophosphate: in situ observations by scanning force microscopy. *Geochim. Cosmochim. Acta* **57,** 705–714.

Fulghum J. E., Bryan S. R., Linton R. W., Bauer C. F., and Griffis D. P. (1988) Discrimination between adsorption and coprecipitation in aquatic particle standards by surface analysis techniques: Lead distributions in calcium carbonates. *Environ. Sci. Tech.* **22,** 463–467.

Fuller C. C. and Davis J. A. (1987) Processes and kinetics of Cd^{2+} adsorption by a calcareous aquifer sand. *Geochim. Cosmochim. Acta* **51,** 1491–1502.

Golovchenko J. A., Kaplan D. R., Cowan P. L., and Bedzyk M. J. (1982) Solution to the surface registration problem using X-ray standing waves. *Phys. Rev. Lett.* **49,** 560.

Gratz A. J., Hillner P. E., and Hansma P. K. (1993) Step dynamics and spiral growth on calcite. *Geochim. Cosmochim. Acta* **57,** 491–495.

Hillner P. E., Manne S., Gratz A. J., and Hansma P. K. (1992) Atomic-scale imaging of calcite growth and dissolution in real time. *Geology* **20,** 359–362.

Hochella M. F., Jr. (1990) Atomic structure, microtopography, composition, and reactivity of mineral surfaces. In *Mineral-Water In-*

terface Geochemistry (ed. M. F. Hocehlla, Jr. and A. F. White); *Rev. Mineral.* **23,** 87–132.

Hochella, M. F., Jr. (1995) Mineral surfaces: their characterization and their chemical, physical and reactive nature. In *Mineral Surfaces* (ed. D. J. Vaughan and R. A. D. Pattrick), pp. 17–60. Chapman and Hall.

Hochella M. F., Jr., and White A. F., ed. (1990) *Mineral-Water Interface Geochemistry. Rev. Mineral.* **23.**

Kendelewicz T., Liu P., Labiosa W. B., and Brown G. E., Jr. (1995) Surface EXAFS and X-ray standing wave study of the cleaved CaO(100) surface. *Physica B* **208/209,** 441–442.

Liang Y., Lea A. S., Baer D. R., and Engelhard M. H. (1996) Structure of the cleaved $CaCO_3$ (104) surface in an aqueous environment. *Surface Sci.* **351,** 172–182.

Lorens R. B. (1981) Strontium, cadmium, manganese, and cobalt distribution coefficients in calcite as a function of calcite precipitation rate. *Geochim. Cosmochim. Acta* **45,** 553–561.

Manceau A., Charlet L., Boisset M. C., Dider B., and Spadin L. (1992) Sorption of heavy metals on hydrous Fe and Mn oxides. *Appl. Clay Sci.* **7,** 201–223.

Manceau A. et al. (1996) Direct determination of lead speciation in contaminated soils by EXAFS spectroscopy. *Environ. Sci. Tech.* **30,** 1540–1552.

McBride M. B. (1980) Chemisorption of Cd^{2+} on calcite surfaces. *Soil Sci. Amer. J.* **44,** 26–28.

Nowack B. and Sigg L. (1996) Adsorption of EDTA and EDTA-metal complexes onto goethite. *J. Colloid Interface Sci.* **177,** 106–121.

Nriagu J. O. ed. (1978) *The Biogeochemistry of Lead in the Environment.* Elsevier.

Ohnesorge F. and Binnig G. (1993) True atomic resolution by atomic force microscopy through attractive and repulsive forces. *Science* **260,** 1451–1456.

Pickering W. F. (1983) Extraction of copper, lead, zinc, and cadmium ions adsorbed on calcium carbonate. *Water, Air, Soil Pollution* **20,** 299–309.

Pingitore N. E., Lytle F. W., Davies B. M., Eastman M. P., Eller P. G., and Larson E. M. (1992) Mode of incorporation of Sr^{2+} in calcite: Determination by X-ray absorption spectroscopy. *Geochim. Cosmochim. Acta* **56,** 1531–1538.

Qian Y., Sturchio N. C., Chiarello R. P., Lyman P. F., Lee T. L., and Bedzyk M. J. (1994) Lattice location of trace elements within minerals and at their surfaces with X-ray standing waves. *Science* **265,** 1555–1557

Reeder R. J. (1983) Crystal chemistry of the rhombohedral carbonates. In *Carbonates: Mineralogy and Chemistry* (ed. R. J. Reeder); *Rev. Mineral.* **11,** 1–47.

Reeder R. J. (1996) Interaction of divalent cobalt, zinc, cadmium, and barium with the calcite surface during layer growth. *Geochim. Cosmochim. Acta* **60,** 1543–1552.

Reeder R. J., Lamble G. M., Lee J.-F., and Staudt W. J. (1994) Mechanism of SeO_4^{2-} substitution in calcite: An XAFS study. *Geochim. Cosmochim. Acta* **58,** 5639–5646.

Robinson I. M. (1986) Crystal truncation rods and surface roughness. *Phys. Rev. B* **33,** 3830–3836.

Roe A. L., Hayes K. F., Chisholm-Brause C. J., Brown G. E., Jr., Parks G. A., and Leckie J. (1991) X-ray absorption study of lead complexes at α-FeOOH/water interfaces. *Langmuir* **7,** 367–373.

Stipp S. L. S. and Hochella M. F., Jr. (1991) Structure and bonding environments at the calcite surface as observed with X-ray photoelectron spectroscopy (XPS) and low energy electron diffraction. *Geochim. Cosmochim. Acta* **55,** 1723–1736.

Stipp S. L. S., Hochella M. F., Jr., Parks G. A., and Leckie J. O. (1992) Cd^{2+} uptake by calcite, solid-state diffusion, and the formation of solid-solution: Interface processes observed with near-surface sensitive techniques (XPS, LEED, and AES). *Geochim. Cosmochim. Acta* **56,** 1941–1954.

Stipp S. L., Eggleston C. M., and Nielsen B. S. (1994) Calcite surface structure observed at microtopographic and molecular scales with atomic force microscopy (AFM). *Geochim. Cosmochim. Acta* **58,** 3023–3033.

Stumm W. (1992) *The Solid-Water Interface.* Wiley.

Stumm W. and Morgan J. (1981) *Aquatic Chemistry,* 2nd ed. Wiley.

Sverjensky D. A. (1984) Prediction of Gibbs free energies of calcite-type carbonates and the equilibrium distribution of trace elements between carbonates and aqueous solutions. *Geochim. Cosmochim. Acta* **48,** 1127–1134.

Sverjensky D. A. and Molling P. A. (1992) A linear free energy relationship for crystalline ions and aqueous solutions. *Nature* **356,** 231–134.

Tesoriero A. J. and Pankow J. F. (1996) Solid-solution partitioning of Sr^{2+}, Ba^{2+}, and Cd^{2+} to calcite. *Geochim. Cosmochim. Acta* **60,** 1053–1063.

Toney M. F. et al. (1994) Voltage-dependent ordering of water molecules at an electrode-electrolyte interface. *Nature* **368,** 444–446.

Towle S. N. et al. (1993) Grazing-incidence EXAFS spectroscopy of metal ion sorption on single-crystal α-Al_2O_3. 205th American Chemical Society National Meeting, Denver, CO, USA (abstr.)

Vaughan D. J. and Pattrick R. A. D., ed. (1995) *Mineral Surfaces.* Chapman and Hall.

Wang J., Bedzyk M. J., Penner T. L., and Caffrey M. (1991) Structural studies of membranes and surface layers up to 1,000 Å thick using X-ray standing waves. *Nature* **354,** 377–379.

Wouters L. C., Van Grieken R. E., Linton R. W., and Bauer C. F. (1988) Discrimination between coprecipitated and adsorbed lead on individual calcite particles using laser microprobe mass analysis. *Anal. Chem.* **60,** 2218–2220.

Xu N. (1993) Spectroscopic and solution chemistry studies of cobalt(II) sorption mechanisms at the calcite-water interface. Ph.D. dissertation, Stanford Univ.

Yee D. (1995) In situ surface X-ray diffraction studies of electrochemically deposited monolayers. Ph.D. dissertation, Univ. Washington.

Zachara J. M., Kittrick J. A., and Harsh J. B. (1988) The mechanism of zinc adsorption on calcite. *Geochim. Cosmochim. Acta* **52,** 2281–2291.

Zachara J. M., Cowan C. E., and Resch C. T. (1991) Sorption of divalent metals on calcite. *Geochim. Cosmochim. Acta* **55,** 1549–1562.